RESEARCH ARTICLE
ATMOSPHERIC PHYSICS

Earth and Planetary Physics
10: 463–471, 2026
doi: 10.26464/epp2026037

The influence of quasi-2-day waves on the transport of CO_2 based on WACCM-NEDAS data assimilation

Sheng-Yang Gu[1,2*], XiaoLong Wang[1], Hao Chen[1], YuXuan Liu[1], and YuSong Qin[1]

[1]School of Earth and Space Science and Technology, Wuhan University, Wuhan 430072, China;

[2]Wuhan Institute of Quantum Technology, Wuhan 430072, China

Key Points:

- Quasi-2-day waves (Q2DWs) in the mesopause region are reproduced well by the newly developed Whole Atmosphere Community Climate Model (WACCM) + Next-generation Ensemble Data Assimilation System (NEDAS).
- The carbon dioxide (CO_2) concentration also shows a clear Q2DW mainly resulting from the Q2DW temperature perturbations.
- Enhancement of the CO_2 vertical gradients induced by vertical motion during the sudden stratospheric warming period also contributes to the strengthened Q2DW in CO_2.

Citation: Gu, S.-Y., Wang, X. L., Chen, H., Liu, Y. X., and Qin, Y. S. (2026). The influence of quasi-2-day waves on the transport of CO_2 based on WACCM-NEDAS data assimilation. *Earth Planet. Phys.*, *10*(3), 463–471. http://doi.org/10.26464/epp2026037

Abstract: The distribution and transport of carbon dioxide (CO_2) in the middle and upper atmosphere are closely linked to atmospheric dynamical processes, but the influence of planetary waves on CO_2 transport remains unclear. This study aims to investigate the impact of quasi-2-day waves (Q2DWs) on CO_2 transport in the stratosphere–mesosphere during the sudden stratospheric warming (SSW) period. On the basis of data assimilation (DA) using the Whole Atmosphere Community Climate Model (WACCM) + Next-generation Ensemble Data Assimilation System (NEDAS) from December 2018 to February 2019, we used the transformed Eulerian mean framework to conduct a diagnostic analysis on Q2DW propagation and amplification. Additionally, we identified unstable regions in the stratosphere between 60°N and 80°N. This configuration facilitates the amplification of Q2DWs through enhanced baroclinic and barotropic instabilities. The results demonstrate that the dynamic features exhibit distinct propagation and amplification characteristics. We also found distinct Q2DWs in CO_2 at the middle latitudes of the southern hemisphere, which were mainly induced by the Q2DWs in temperature. Further analysis showed that the anomalous vertical motion during the SSW period could lead to the enhancement of CO_2 vertical gradients, which also contributed to the strengthening of Q2DWs in CO_2.

Keywords: quasi-2-day wave; sudden stratospheric warming; data assimilation; CO_2 transport

1. Introduction

As a greenhouse gas with an extremely low content in the atmosphere, carbon dioxide (CO_2) exhibits distinct climatological characteristics. Its long atmospheric lifetime, well-mixed distribution from the troposphere to the mesopause, and dominant role in radiative forcing and climate feedback have been confirmed by extensive observations, paleoclimatic studies, and model simulation studies (e.g., Keeling et al., 1976; Andrews et al., 1987; Conway et al., 1994; Lüthi et al., 2008; Lacis et al., 2010; Solomon et al., 2010; Bereiter et al., 2015; Etminan et al., 2016; Friedlingstein et al., 2019). Since the Industrial Revolution, the atmospheric concentration of CO_2 has increased from ~280 ppm to ~420 ppm (an increase of nearly 50%), and this rapid change has become a central driver of global climate change (Friedlingstein et al., 2019). The spatial distribution of CO_2 in the atmosphere shows distinct seasonal and interannual variations. Carbon dioxide concentrations exhibit a clear seasonal cycle, with higher levels generally observed in the winter months and lower levels in summer, largely because of seasonal changes in vegetation, oceanic uptake, and atmospheric dynamics (Zhang X et al., 2007). Interannually, CO_2 levels fluctuate in response to events such as the El Niño–Southern Oscillation, which influences the tropical convection and subsequently alters CO_2 distribution in the upper troposphere (Wang J et al., 2018; Wade et al., 2023). However, the characteristics of short-term CO_2 variations remain unclear at present.

Sudden stratospheric warming (SSW) is a large-scale disturbance in the stratosphere during winter, typically attributed to the breaking of stationary planetary waves (PWs; e.g., Andrews et al., 1987; Butler et al., 2015). During an SSW event, the temperature in the polar stratosphere rises by several tens of kelvins within one week. Sudden stratospheric warming events are accompanied by a weakening of the polar vortex and may also be associated with an uplift of the stratopause (Miller et al., 2013; Vignon and Mitchell, 2015). Unlike long-term variations, SSW events significantly modulate the distribution of CO_2 in the middle and upper

Correspondence to: S. Y. Gu, gushengyang@whu.edu.cn
Received 10 DEC 2025; Accepted 02 FEB 2026.
First Published online 17 MAR 2026.

atmosphere over the short term by altering large-scale circulation, vertical transport, and wave–mean flow interactions, which in turn lead to notable anomalies in CO_2 mixing ratios from the stratopause to the lower thermosphere (Shepherd et al., 2014; Kumar et al., 2025). Additionally, SSW events play a substantial role in modulating the transport processes in the atmosphere by influencing the dynamical processes of the middle and upper atmosphere. Strong wind shear can cause abnormal behaviors of PWs by enhancing atmospheric instability during the SSW period (e.g., Matsuno, 1971; Belova et al., 2009; Baldwin et al., 2021; Park et al., 2024; Zhang CY et al., 2024; Yoo and Chun, 2025). These instabilities enhance the upward transport and vertical displacement of trace gases, including CO_2, within the stratosphere (Tassev et al., 1993; Shepherd et al., 2008). The occurrence of an SSW event is closely linked to the amplification and breaking of PWs, which serve as an important mechanism for redistributing energy and momentum in the middle atmosphere (Yoshida and Yamazaki, 2011).

Periodic oscillations also affect the distribution of CO_2. Planetary waves, also known as Rossby waves, are one kind of large-scale periodic oscillations. These global-scale oscillations arise from the latitudinal variation of the Coriolis parameter and play a central role in shaping the dynamical structure of the middle atmosphere (e.g., Charney and Drazin, 1961; Andrews et al., 1987; Shepherd, 2007; Holton and Hakim, 2013; Vallis, 2017; Yasui et al., 2021). The middle and upper atmosphere, as a special resonant system, produces a spectrum of normal modes, including the well-known quasi-2-day, quasi-4-day, quasi-6-day, and quasi-10-day oscillations, which represent intrinsic large-scale dynamical responses of the atmosphere (e.g., Forbes, 1995; Salby and Callaghan, 2001; Madden, 2007; Yamazaki et al., 2021). Among these normal (unforced) modes, the quasi-2-day wave (Q2DW) is the most prominent during the northern hemisphere winter. The Q2DW is a high-frequency, large-scale oscillation that typically exhibits strong amplitudes in the tropical stratosphere, propagates poleward and upward, and thereby modulates the temperature and wind fields (Gu SY et al., 2015; Iimura et al., 2021). Carbon dioxide is an excellent tracer in the atmosphere, and analyzing Q2DWs in the CO_2 mixing ratio provides a feasible way to investigate its short-term variability.

A significant SSW event occurred in December 2018, and Q2DWs were observed during this SSW period. This study investigates the origin of this dynamical phenomenon and its influence on the transport of CO_2. In this article, Section 2 presents the data and methods, and Section 3 shows the results and discussion. A summary is provided in Section 4.

2. Data and Methods

2.1 Data

In this study, we use model simulation data to investigate the transport and variability of CO_2 in the middle and upper atmosphere. The simulations were performed by data assimilation (DA), which was developed by coupling the Next-generation Ensemble Data Assimilation System (NEDAS) with the Whole Atmosphere Community Climate Model (WACCM). The system assimilates multi-platform temperature and wind observations (e.g., NCEP PrepBUFR [National Centers for Environmental Prediction Prepared data in Binary Universal Form for the Representation of meteorological data], TIMED [Thermosphere Ionosphere Mesosphere Energetics and Dynamics]/SABER [Sounding of the Atmosphere using Broadband Emission Radiometry], Aura MLS [Aura Microwave Limb Sounder], COSMIC [Constellation Observing System for Meteorology, Ionosphere, and Climate]) from the troposphere to the lower thermosphere by using the Local Ensemble Transform Kalman Filter. Data assimilation extends from the surface to the lower thermosphere (70 pressure levels, ~0–140 km) and includes fully interactive chemistry and dynamics, making it suitable for studying processes that influence CO_2 distribution. The model was run with a horizontal resolution of 1.9° latitude × 2.5° longitude, covering December 2018 to February 2019. Model outputs of the zonal wind (u), meridional wind (v), vertical velocity (w), air density (ρ), geopotential height (GPH), temperature (T), and CO_2 volume mixing ratio were archived at 1-hour intervals for analysis.

For detailed information about the DA, please refer to Liu YX et al. (2025). This study assesses the adopted dataset through comparative analysis with outputs from several independent models and corresponding observational records. The results demonstrate that the DA system provides an accurate representation of PW dynamics and successfully captures SSW events. As demonstrated in Figures 10 and 11 of Liu YX et al. (2025), the DA system effectively reproduces the responses of chemical constituents to PW activity during SSW episodes. These findings substantiate the robustness and reliability of the dataset utilized in this study.

2.2 Method

For datasets containing longitudinal information, the PWs are extracted using least-squares fitting applied to the following equation (Wu DL et al., 1995):

$$y_i = A\cos\left[2\pi\left(\sigma t_i + s\lambda_i\right)\right] + B\sin\left[2\pi\left(\sigma t_i + s\lambda_i\right)\right] + C. \tag{1}$$

Among them, y_i represents the measured value of the ith data point; t_i denotes the time at which this data point is recorded; λ_i is the longitude of the location where this data point is situated; σ and s represent the frequency and zonal wavenumber of the wave, respectively (with westward propagation denoted as positive); and A, B, and C are the results to be obtained through fitting, which represent the amplitude ($\sqrt{A^2+B^2}$) of the trigonometric function and the atmospheric background value (zonal mean value), respectively.

To examine the dynamical modulation of CO_2, perturbation components (v', w', and χ') are derived by removing the zonal mean from the total fields. The evolution of CO_2 perturbations associated with planetary-scale waves is described using the linearized continuity equation for a conservative tracer (Limpasuvan and Wu DL, 2003; Andrews et al., 1987):

$$\left(\frac{\partial}{\partial t} + \overline{u}\frac{\partial}{\partial x}\right)\chi' + v'\overline{\chi}_y + w'\overline{\chi}_z = 0, \tag{2}$$

where χ' denotes the CO_2 perturbation, and v' and w' represent the PW perturbations in meridional and vertical winds, respec-

tively. The second and third terms describe the contributions of the meridional advection ($v'\overline{\chi}_y$) and vertical transport ($w'\overline{\chi}_z$) to perturbations of the tracer, which are key processes driving CO_2 variability during Q2DW events. Assuming waves have the form of $\cos[2\pi(\sigma t + k\lambda)]$, where k is the wavenumber and σ is the frequency, Equation (1) can be written as follows:

$$-\mathrm{i}2\pi\left(\sigma + k\overline{u}\right)\chi' + v'\overline{\chi}_y + w'\overline{\chi}_z = 0. \tag{3}$$

For a certain planetary-scale wave like the Q2DW, the perturbation in CO_2 is determined by the second term in Equation (3), meridional advection, and the third term, vertical transport. The PW disturbances in temperature (T'), zonal wind (u'), meridional wind (v'), and vertical wind (w') are often determined by their dispersion relations derived from the linearized primitive equations in a spherical atmosphere (Andrews et al., 1987). Equation (3) indicates that the perturbation in CO_2 is highly dependent on the vertical and meridional gradients.

Similar to Equation (3), the linearized wave temperature equations assume no diabatic processes (Andrews et al., 1987; Yue J and Gan Q, 2021):

$$-\mathrm{i}2\pi\left(k\overline{u} + \sigma\right)T' + w'S = 0, \tag{4}$$

where S is static stability $S = \left(\frac{\partial T}{\partial z} + \frac{g}{c_p}\right)$, g is the acceleration of gravity, and c_p is the heat capacity at constant pressure. The second term denotes adiabatic cooling or warming associated with the vertical motion (Yue J and Gan Q, 2021). From Equations (3) and (4), we can relate the CO_2 perturbation χ' to the temperature perturbation T'. Assuming the meridional term is small, a simple relationship can be derived (Smith et al., 2010; Yue J and Gan Q, 2021):

$$\chi' = \frac{\overline{\chi}_z}{S}T'. \tag{5}$$

When studying the background zonal wind field and temperature variations, it is necessary to determine the values of the residual circulation. The meridional and vertical residual circulation values can be defined by the following two formulas (Andrews et al., 1987):

$$\overline{v}^* \equiv \overline{v} - \frac{1}{\rho}\left(\frac{\rho\overline{v'\theta'}}{\overline{\theta}_z}\right)_z, \tag{6}$$

$$\overline{w}^* \equiv \overline{w} + \frac{\left(\frac{\cos\Phi\overline{v'\theta'}}{\overline{\theta}_z}\right)_\Phi}{a\cos\Phi}, \tag{7}$$

where ρ is the atmospheric density, θ' is the potential temperature perturbation, a represents the Earth's radius, and Φ is the latitude. The overbar indicates the zonal mean, whereas the subscripts indicate the latitudinal (Φ) and vertical (z) gradients.

The Eliassen–Palm (EP) flux divergence (EPFD) of PWs, also known as PW drag, has positive and negative values that can represent the sources and sinks of PWs, respectively. The EP flux of PWs (0, $F^{(\Phi)}$, $F^{(z)}$)(with its meridional component abbreviated as EPY and vertical component abbreviated as EPZ) is determined by the following formulas (Palmer, 1982; Andrews et al., 1987):

$$F^{(\Phi)} = \rho a\cos\Phi\left(\frac{\overline{u_z}\overline{v'\theta'}}{\overline{\theta}_z} - \overline{v'u'}\right), \tag{8}$$

$$F^{(z)} = \rho a\cos\Phi\left\{\left[f - \frac{\left(\overline{u}\cos\Phi\right)_\Phi}{a\cos\Phi}\right]\frac{\overline{v'\theta'}}{\overline{\theta}_z} - \overline{w'u'}\right\}, \tag{9}$$

$$\nabla\cdot\boldsymbol{F} = \frac{1}{a\cos\Phi}\frac{\partial}{\partial\Phi}\left(F^{(\Phi)}\cos\Phi\right) + \frac{\partial F^{(z)}}{\partial z}. \tag{10}$$

For PWs, their propagation and amplification are primarily controlled by critical layers (CLs), various instabilities of the background atmosphere, and planetary waveguides. The CL of a PW is the region where the zonal mean wind equals the phase speed of the wave (i.e., $\overline{u} - c_x = 0$). The phase speed of the PW is determined by the following formula:

$$c_x = -\frac{2\pi a\sigma}{s}\cos\Phi. \tag{11}$$

The latitudinal gradient of the quasi-geostrophic potential vorticity is expressed as

$$\overline{q}_\Phi = 2\Omega\cos\Phi - \left(\frac{\left(\overline{u}\cos\Phi\right)_\Phi}{a\cos\Phi}\right)_\Phi - \frac{a}{\rho}\left(\frac{f^2}{N^2}\rho\overline{u}_z\right)_z, \tag{12}$$

where f is the Coriolis force parameter ($f = 2\Omega\sin\Phi$, where Ω represents the Earth's rotational velocity) and N represents the Brunt–Väisälä frequency. In the background atmosphere, the region where $\overline{q}_\Phi < 0$ is the area where atmospheric baroclinic and barotropic instabilities exist. Within this region, PWs can absorb energy from wave–mean flow interactions and thus be amplified (Meyer and Forbes, 1997).

3. Results and Discussion

Figures 1a–1d compare the Q2DW derived from Aura MLS observations and DA. Figures 1a and 1c show the spectra of the westward zonal wavenumber 3 (W3) component at ~40°S and 85 km. The Q2DWs in both datasets exhibit a dominant period of ~46 hours, with the Q2DW activities intensifying from late December and peaking around January 20. Figures 1b and 1d display the latitude –altitude cross sections on January 20, 2019. In the latitude–altitude cross sections, both datasets show strong temperature perturbations centered at ~40°S and ~80 km, indicating that the assimilation reproduces the observed spatial structure of the Q2DW.

Figure 1e shows the zonal wind (u), whereas the shading indicates the potential vorticity gradient ($\overline{q}_\Phi$) and CLs. From January 16 to 23, 2019, an unstable region (where $\overline{q}_\Phi < 0$) appeared at 60°–80°N in the stratosphere (red box in Figure 1e), caused by enhanced vertical shear during the SSW event. Meanwhile, a significant positive EPFD occurred in the middle latitudes of the southern hemisphere (Figure 1g). This configuration favored the amplification of the Q2DW by baroclinic and barotropic instabilities of the easterly jet. Figure 1f shows the EP flux vectors of W3 Q2DW on January 20, 2019. The W3 Q2DW shows a strong upward component of the EP flux vectors in the middle to low latitudes of the southern hemisphere above 80 km. The CL of the W3 Q2DW in the mesosphere over the middle to low latitudes in the southern hemisphere passes through the unstable region of the atmosphere, as shown

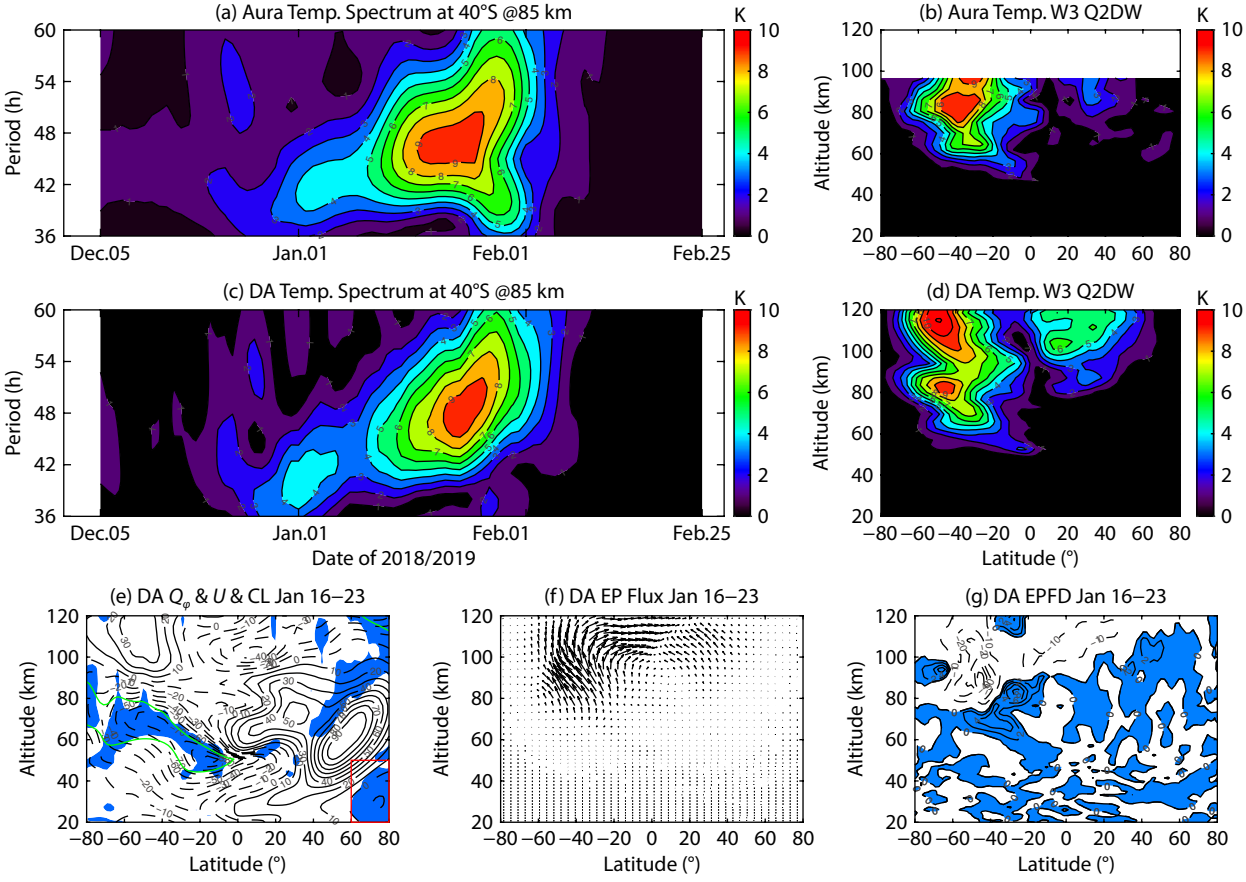

Figure 1. (a) Westward zonal wavenumber 3 (W3) Q2DW spectrum at 40°S and 85 km of the Aura MLS temperature. (b) Q2DW latitude–altitude cross sections on January 20, 2019, of the Aura MLS temperature. (c, d) Similar to (a) and (b) but for the DA temperature. (e) Zonal mean zonal wind (U, contours, m/s), the unstable areas of the atmosphere ($\overline{q}_\phi < 0$, blue shading), and critical layers (CLs) for January 16–23, 2019. (f) Eliassen–Palm (EP) flux of Q2DW (46 hours) for January 16–23, 2019. (g) EP flux divergence (EPFD, normalized) of Q2DW (46 hours) for January 16–23, 2019. The shaded region indicates positive EPFD, and the contour intervals are 2 m/s per day (shaded region) and 10 m/s per day (white region).

in Figure 1e. Therefore, the W3 Q2DW in the DA is amplified through wave–mean flow interaction, which is consistent with previous studies (e.g., Gu SY et al., 2016, 2018).

According to the results shown in Figure 1, the DA can effectively simulate the variations in the background atmospheric state and the excitation, propagation, and amplification of the Q2DW. Hence, DA can reliably be used to study the role of the Q2DW in the transport of photochemical components and the impact of dynamical processes during the SSW event on this transport.

Because the Q2DW can induce oscillations in temperature and winds, chemical constituents can be modulated by the wave through chemical production or loss, advective transport, and so forth. As illustrated in Figure 2, a periodic oscillation is clearly discernible in the CO_2 mixing ratio observations. Notably, the latitudinal structure presented in Figure 2a exhibits a close correspondence to the canonical characteristic pattern of the Rossby–gravity (3, 0) mode, with its latitudinal and vertical distributions aligning well with the theoretical and observational benchmarks of this PW type (Salby, 1981; Huang YY et al., 2013). Furthermore, the temporal variability and spatial evolution of this Q2DW show a high degree of consistency with those of the dynamically driven ones, as quantified by temperature perturbations, which is a well-established tracer for dynamical Q2DW activities in the middle atmosphere (Lainer et al., 2018; Yue J and Gan Q, 2021). This strong congruence in both temporal phase coherence and spatial structure supports the notion that the PW signature observed in the CO_2 mixing ratio is likely linked to fundamental atmospheric dynamical processes. Specifically, the alignment suggests that Q2DW-induced dynamical perturbations (e.g., wave-driven meridional and vertical circulation) may modulate the distribution of atmospheric CO_2 by altering transport pathways or the mixing efficiency in the middle atmosphere, thereby imprinting the characteristic pattern of the wave onto the CO_2 mixing ratio. It thus suggests that the PW detected in CO_2 is intimately associated with the underlying dynamical mechanisms governing Q2DW generation and propagation in the middle atmosphere.

Figures 3b and 3c display the assimilation CO_2 mixing ratio and its meridional gradient $\overline{\chi_y}$ and vertical gradient $\overline{\chi_z}$. In the troposphere and lower mesosphere, because of the well-mixed atmosphere, the mixing ratio of CO_2 is basically constant with height. When the altitude increases to ~80 km or above (near the mesopause),

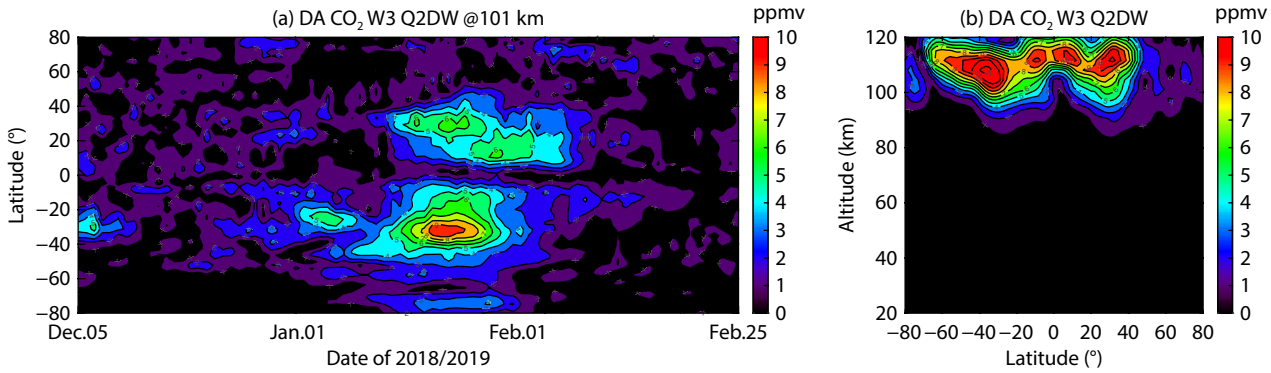

Figure 2. (a) Latitude–time distribution of the W3 Q2DW CO_2 perturbations at 101 km from December 2018 to February 2019. (b) Latitude–altitude cross-section of the W3 Q2DW (46-hour) amplitude. The results in Figure 2 are calculated by DA.

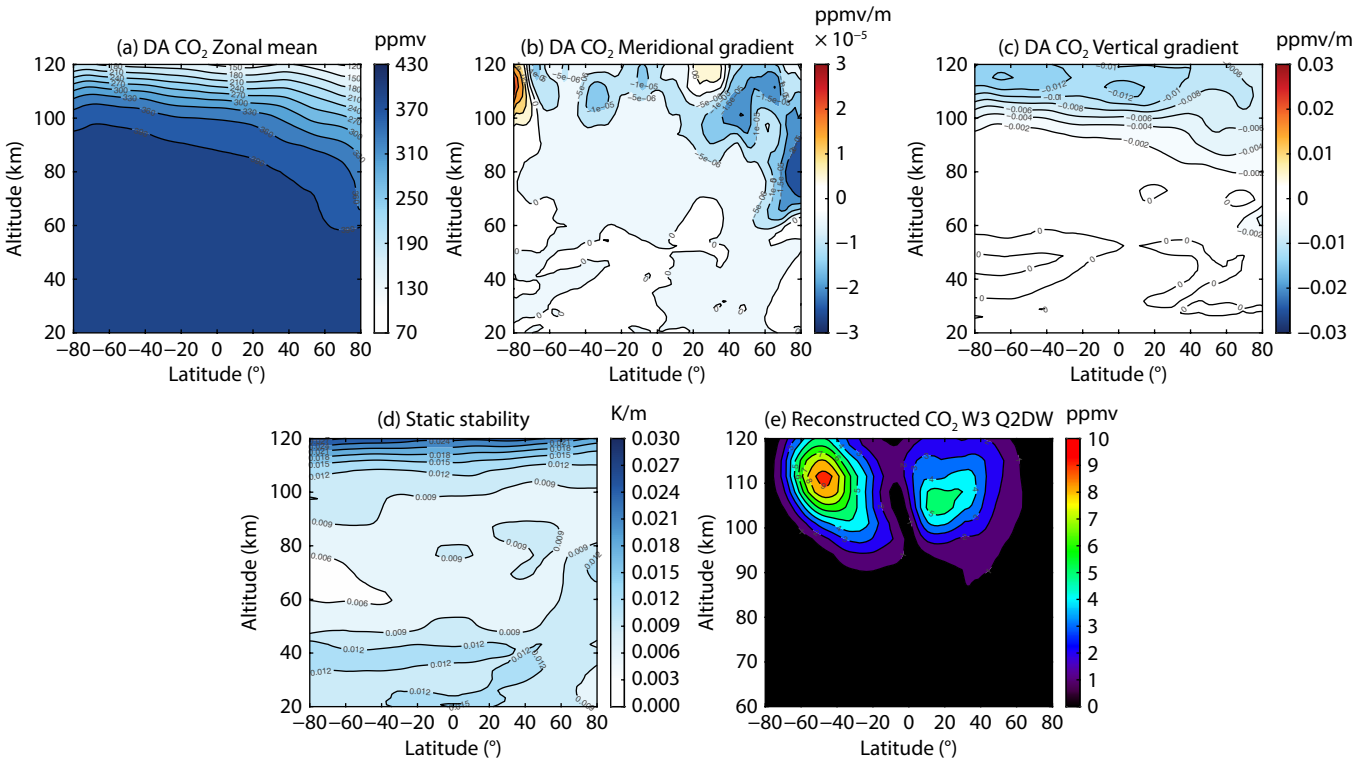

Figure 3. (a) Zonal mean CO_2 distribution. (b) Meridional CO_2 gradient. (c) Vertical CO_2 gradient. (d) Static stability (S). (e) Reconstructed W3 Q2DW CO_2 amplitude. The results in Figure 3 are calculated by using DA from January 16 to 23, 2019.

molecular diffusive separation and photolysis lead to a decrease with increasing altitude of the CO_2 mixing ratio (Rezac et al., 2015). Therefore, we can see the different layers of the CO_2 mixing ratio decreasing with the altitude uplift at 80–120 km in Figure 3a. Almost no change occurs below 80 km. In addition, the CO_2 vertical gradient is strongest near 110 km at all latitudes at approximately 12 ppmv/km and is very small below 90 km. This result explains that the Q2DW in CO_2 is absent below 90 km in Figure 2b. The meridional gradient is much smaller, especially at low latitudes, as displayed in Figure 2b. In the middle- and high-latitude regions between 90 and 120 km, the gradient is as large as 2×10^{-3} ppmv/km. Those meridional gradients are caused by large-scale atmospheric circulation, upwelling in the polar regions, and sinking toward the equatorial regions (Rezac et al., 2015).

Although the vertical gradient of CO_2 is large at all latitudes (Figure 3c), the meridional gradient is significant only at the middle to high latitudes (Figure 3b) and is ~1000 times smaller than the vertical gradient. Therefore, it is reasonable to ignore the meridional term at low latitudes in Equation (3). Perturbation in vertical transport can be derived from temperature perturbation, as shown in Equation (4). Therefore, we can reconstruct the Q2DW perturbation in CO_2 from the temperature data. This is referred to as the adiabatic displacement approach (Yue J and Gan Q, 2021).

Through Equation (5), we reconstructed the Q2DW in CO_2 from only vertical transport. This equation is valid at the low and middle latitudes, where the CO_2 meridional gradient is much smaller than the vertical one. The perturbation of CO_2 χ' has a linear relationship with the temperature perturbation T', and the

proportional coefficient is jointly determined by the CO_2 vertical gradient $\overline{\chi_z}$ and the static stability S of the background atmosphere. Static stability S determines the intensity of the response of CO_2 in the upper atmosphere to temperature perturbations (Rezac et al., 2015). Above the mesopause, where S is relatively small and the vertical gradient of CO_2 is steeper, the response of CO_2 to PWs is more pronounced. In the lower atmosphere (the region with high S), the vertical mixing of CO_2 is sufficient, which suppresses perturbations.

Figure 3d shows the static stability with a minimum of 5 K/km between 70 and 90 km. The static stability is relatively weaker at low latitudes, whereas it becomes stronger at high latitudes, especially in the upper atmosphere of the northern hemisphere. A stronger vertical gradient of ~12 ppmv/km of CO_2 appears around 110 km as well (Figure 3c). This is because the small S makes CO_2 more prone to vertical transport, whereas the waves are more likely to cause CO_2 concentration perturbations and local temporal variations. A comparison of Figures 2b and 3e indicates that the reconstructed CO_2 perturbation derived from the temperature field by using Equation (4) reproduces the main spatial features of the assimilated CO_2 field in the mesosphere and lower thermosphere region. Both distributions exhibit two pronounced maxima around ±40° latitude near 110 km altitude, corresponding to the regions of enhanced wave activity. The amplitude is in good agreement, indicating that the CO_2 perturbations are primarily driven by temperature variations through vertical transport modulated by the background static stability. Minor discrepancies between the two panels may have resulted from the involvement of photochemical reactions, from nonlinear processes not captured in the linear approximation, and from differences in the data themselves.

According to Figure 1, the Q2DW in temperature was relatively strong in the middle of January 2019, and the SSW event may have further amplified this PW. Equation (5) shows that the perturbation in chemical composition is proportional to the vertical gradient of the chemical composition and the temperature perturbation and is inversely proportional to the static stability. As the SSW event causes stratopause uplift (Figure 4c), the enhanced upward flow transports the CO_2-rich air from lower levels to higher levels, resulting in an increase in the vertical gradient of CO_2 in the upper atmosphere. As shown in Figure 4a, the zonal mean concentration of CO_2 exhibits a significant upwelling after the SSW event. This leads to an increase in the vertical gradient of CO_2 at higher altitudes, as presented in Figure 4b. The deceleration, reversion, or both of the eastward zonal wind in the stratosphere enables the propagation of more eastward gravity waves upward into the mesosphere, which transmits eastward momentum fluxes to the background mean flow and consequently southward and upward circulation in the polar mesospheric regions resulting from the Coriolis force (Karlsson et al., 2009; Körnich and Becker, 2010; Gu SY et al., 2020). This enhancement of the upward component of the residual circulation during the SSW period is shown in Figure 4d.

4. Summary

Recently, a new middle-atmosphere DA model, WACCM + NEDAS, was developed at Wuhan University. It was found that PWs could be reproduced well by the WACCM + NEDAS, including the Q2DW, which is the most sensitive to changes in the background wind. Analysis of the assimilation datasets showed that the amplitude of this Q2DW in temperature was ~10 K during the 2019 boreal winter, and it was relatively strong in the middle latitudes of the southern hemisphere, which agrees well with Aura MLS observations. In addition, a Q2DW in CO_2 was detected with an amplitude of ~10 ppmv. We compared the Q2DW perturbations in temperature with those in CO_2 and found that they exhibited good consistency in spatial and temporal variations, which was particularly prominent in the middle latitudes of the southern hemisphere.

Theoretically, the Q2DW in the CO_2 mixing ratio is mainly driven by the combined effects of vertical transport and meridional advection, as well as the Q2DW perturbations, among which the role of vertical transport is more crucial in the low to middle latitudes. Our analysis showed that the Q2DW in CO_2 can be primarily restructured by the combined effect of temperature perturbations and CO_2 vertical gradients. Furthermore, we found that the vertical gradients of CO_2 increased because of the vertical component anomaly of the residual circulation, which was related to the change in gravity wave breaking in the mesopause region during an SSW event. The enhancement of the vertical gradient in CO_2 also contributes to the amplification of the Q2DW of CO_2 related to the Q2DW event.

The interpretation of results can be explained by the following two characteristics. First, the SSW event causes the stratopause to lift, which enhances the vertical transport of CO_2 and thereby leads to an increase in the vertical gradient of CO_2. Second, the Q2DW originates in the Arctic stratosphere and is subsequently amplified by the barotropic and baroclinic instabilities in the southern hemisphere mesosphere. Additionally, the enhanced wind shear in the Arctic stratosphere during the SSW period exerts a certain amplifying effect on the Q2DW.

Future work will further quantify the impact of OH and O_3 on CO_2 oscillations by using photochemical models and will expand the statistical analyses under non-SSW conditions to refine the framework of dynamical driving mechanisms for stratospheric–mesospheric atmospheric chemical components.

Acknowledgments

This research was supported by the National Natural Science Foundation of China (Grant Nos. 42374195, 42404168, and 42188101), a fellowship from the China National Postdoctoral Program for Innovative Talents (Grant No. BX20230273), the Hubei Provincial Natural Science Foundation of China (Grant No. 2024AFB097), and the Postdoctoral Project of Hubei Province (Grant No. 2024HBBHCXA054).

References

Andrews, D. G., Leovy, C. B., and Holton, J. R. (1987). *Middle Atmosphere Dynamics (Vol. 40)*. Orlando, FL: Academic Press.

Baldwin, M. P., Ayarzagüena, B., Birner, T., Butchart, N., Butler, A. H., Charlton-Perez, A. J., Domeisen, D. I. V., Garfinkel, C. I., Garny, H., ... Pedatella, N. M.

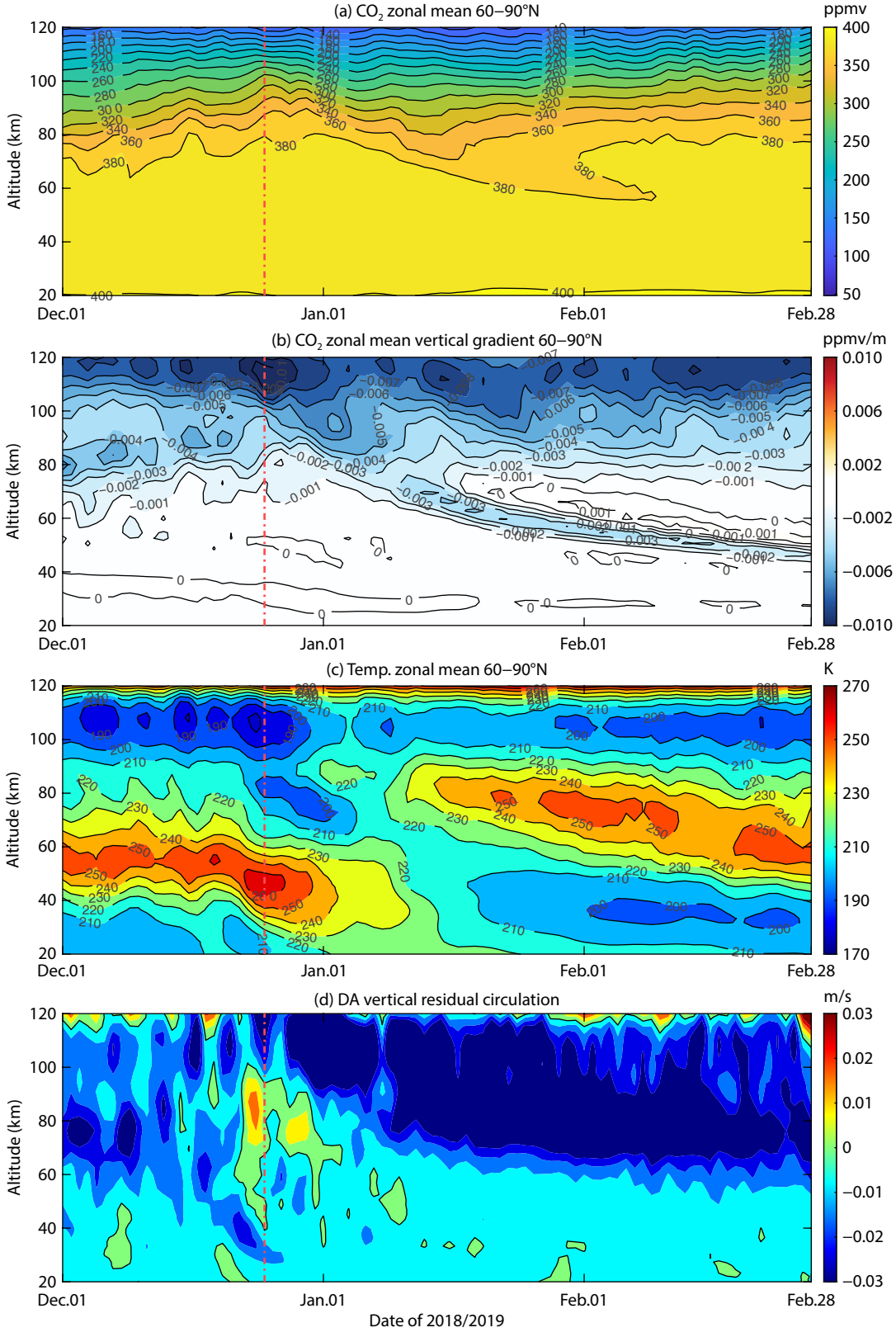

Figure 4. (a) Zonal mean CO_2 distribution. (b) Vertical CO_2 gradient. (c) Zonal mean temperature. (d) Vertical residual circulation (w^*). The dashed red line marks the approximate onset timing of the SSW event. The results in Figure 4 are calculated by DA.

(2021). Sudden stratospheric warmings. *Rev. Geophys.*, *59*(1), e2020RG000708. https://doi.org/10.1029/2020RG000708

Belova, A., Kirkwood, S., and Murtagh, D. (2009). Planetary waves in ozone and temperature in the Northern Hemisphere winters of 2002/2003 and early 2005. *Ann. Geophys.*, *27*(3), 1189–1206. https://doi.org/10.5194/angeo-27-1189-2009

Bereiter, B., Eggleston, S., Schmitt, J., Nehrbass-Ahles, C., Stocker, T. F., Fischer, H., Kipfstuhl, S., and Chappellaz, J. (2015). Revision of the EPICA Dome C CO_2 record from 800 to 600 kyr before present. *Geophys. Res. Lett.*, *42*(2), 542–549. https://doi.org/10.1002/2014GL061957

Butler, A. H., Seidel, D. J., Hardiman, S. C., Butchart, N., Birner, T., and Match, A. (2015). Defining sudden stratospheric warmings. *Bull. Am. Meteor. Soc.*, *96*(11), 1913–1928. https://doi.org/10.1175/BAMS-D-13-00173.1

Charney, J. G., and Drazin, P. G. (1961). Propagation of planetary-scale disturbances from the lower into the upper atmosphere. *J. Geophys. Res.: Space Phys.*, *66*(1), 83–109. https://doi.org/10.1029/JZ066i001p00083

Conway, T. J., Tans, P. P., Waterman, L. S., Thoning, K. W., Kitzis, D. R., Masarie, K. A., and Zhang, N. (1994). Evidence for interannual variability of the carbon cycle from the National Oceanic and Atmospheric Administration/Climate Monitoring and Diagnostics Laboratory global air sampling network. *J. Geophys. Res.: Atmos.*, *99*(D11), 22831–22855. https://doi.org/10.1029/94JD01951

Etminan, M., Myhre, G., Highwood, E. J., and Shine, K. P. (2016). Radiative forcing of carbon dioxide, methane, and nitrous oxide: A significant revision of the methane radiative forcing. *Geophys. Res. Lett.*, *43*(24), 12614–12623. https://doi.org/10.1002/2016GL071930

Forbes, J. M. (1995). Tidal and planetary waves. In R. M. Johnson, et al. (Ed.), *The Upper Mesosphere and Lower Thermosphere: A Review of Experiment and Theory* (pp. 67–87). Washington: American Geophysical Union. https://doi.org/10.1029/GM087p0067

Friedlingstein, P., Jones, M. W., O'Sullivan, M., Andrew, R. M., Hauck, J., Peters, G. P., Peters, W., Pongratz, J., Sitch, S., … Zaehle, S. (2019). Global carbon budget 2019. *Earth Syst. Sci. Data*, *11*(4), 1783–1838. https://doi.org/10.5194/essd-11-1783-2019

Gu, S. Y., Liu, H. L., Li, T., Dou, X. K., Wu, Q., and Russell III, J. M. (2015). Evidence of nonlinear interaction between quasi 2 day wave and quasi-stationary wave. *J. Geophys. Res.: Space Phys.*, *120*(2), 1256–1263. https://doi.org/10.1002/2014ja020919

Gu, S. Y., Liu, H. L., Dou, X. K., and Li, T. (2016). Influence of the sudden stratospheric warming on quasi-2-day waves. *Atmos. Chem. Phys.*, *16*(8), 4885–4896. https://doi.org/10.5194/acp-16-4885-2016

Gu, S. Y., Dou, X. K., Pancheva, D., Yi, W., and Chen, T. D. (2018). Investigation of the abnormal quasi 2-day wave activities during the sudden stratospheric warming period of January 2006. *J. Geophys. Res.: Space Phys.*, *123*(7), 6031–6041. https://doi.org/10.1029/2018JA025596

Gu, S. Y., Hou, X., Qi, J. H., TengChen, K., and Dou, X. K. (2020). Reponses of middle atmospheric circulation to the 2009 major sudden stratospheric warming. *Earth Planet. Phys.*, *4*(5), 472–478. https://doi.org/10.26464/epp2020046

Holton, J. R., and Hakim, G. J. (2013). *An Introduction to Dynamic Meteorology* (5th ed). Amsterdam: Academic Press. https://doi.org/10.1016/C2009-0-63394-8

Huang, Y. Y., Zhang, S. D., Yi, F., Huang, C. M., Huang, K. M., Gan, Q., and Gong, Y. (2013). Global climatological variability of quasi-two-day waves revealed by TIMED/SABER observations. *Ann. Geophys.*, *31*(6), 1061–1075. https://doi.org/10.5194/angeo-31-1061-2013

Iimura, H., Fritts, D. C., Lieberman, R. S., Janches, D., Mitchell, N. J., Franke, S. J., Singer, W., Hocking, W. K., Taylor, M. J., and Moffat-Griffin, T. (2021). Climatology of quasi-2-day wave structure and variability at middle latitudes in the northern and southern hemispheres. *J. Atmos. Sol. Terr. Phys.*, *221*, 105690. https://doi.org/10.1016/j.jastp.2021.105690

Karlsson, B., McLandress, C., and Shepherd, T. G. (2009). Inter-hemispheric mesospheric coupling in a comprehensive middle atmosphere model. *J. Atmos. Sol. Terr. Phys.*, *71*(3-4), 518–530. https://doi.org/10.1016/j.jastp.2008.08.006

Keeling, C. D., Bacastow, R. B., Bainbridge, A. E., Ekdahl, C. A., Guenther, P. R., Waterman, L. S., and Chin, J. F. S. (1976). Atmospheric carbon dioxide variations at Mauna Loa Observatory, Hawaii. *Tellus*, *28*(6), 538–551. https://doi.org/10.3402/tellusa.v28i6.11322

Körnich, H., and Becker, E. (2010). A simple model for the interhemispheric coupling of the middle atmosphere circulation. *Adv. Space Res.*, *45*(5), 661–668. https://doi.org/10.1016/j.asr.2009.11.001

Kumar, A., Sunil Krishna, M. V., and Ranjan, A. K. (2025). A composite of the effects of major sudden stratospheric warming events on carbon dioxide radiative cooling in the mesosphere-lower-thermosphere. *J. Geophys. Res.: Space Phys.*, *130*(7), e2025JA033941. https://doi.org/10.1029/2025JA033941

Lacis, A. A., Schmidt, G. A., Rind, D., and Ruedy, R. (2010). Atmospheric CO_2: principal control knob governing Earth's temperature. *Science*, *330*(6002), 356–359. https://doi.org/10.1126/science.1190653

Lainer, M., Hocke, K., and Kämpfer, N. (2018). Long-term observation of midlatitude quasi 2-day waves by a water vapor radiometer. *Atmos. Chem. Phys.*, *18*(17), 12061–12074. https://doi.org/10.5194/acp-18-12061-2018

Limpasuvan, V., and Wu, D. L. (2003). Two-day wave observations of UARS Microwave Limb Sounder mesospheric water vapor and temperature. *J. Geophys. Res.: Atmos.*, *108*(D10), 4307. https://doi.org/10.1029/2002JD002903

Liu, Y., Gu, S.-Y., Ying, Y., Qin, Y., Chen, H., Wei, Y., and Dou, X. (2025). Application and evaluation of a novel python-based ensemble data assimilation framework NEDAS in whole atmosphere community climate model (WACCM). *ESS Open Archive*. https://doi.org/10.22541/essoar.176097394.402348

Lüthi, D., Le Floch, M., Bereiter, B., Blunier, T., Barnola, J. M., Siegenthaler, U., Raynaud, D., Jouzel, J., Fischer, H., … Stocker, T. F. (2008). High-resolution carbon dioxide concentration record 650,000-800,000 years before present. *Nature*, *453*(7193), 379–382. https://doi.org/10.1038/nature06949

Madden, R. A. (2007). Large-scale, free Rossby waves in the atmosphere—An update. *Tellus A: Dyn. Meteor. Oceanogr.*, *59*(5), 571–590. https://doi.org/10.1111/j.1600-0870.2007.00257.x

Matsuno, T. (1971). A dynamical model of the stratospheric sudden warming. *J. Atmos. Sci.*, *28*(8), 1479–1494. https://doi.org/10.1175/1520-0469(1971)028<1479:ADMOTS>2.0.CO;2

Meyer, C. K., and Forbes, J. M. (1997). A 6.5-day westward propagating planetary wave: Origin and characteristics. *J. Geophys. Res.: Atmos.*, *102*(D22), 26173–26178. https://doi.org/10.1029/97JD01464

Miller, A., Schmidt, H., and Bunzel, F. (2013). Vertical coupling of the middle atmosphere during stratospheric warming events. *J. Atmos. Sol. Terr. Phys.*, *97*, 11–21. https://doi.org/10.1016/j.jastp.2013.02.008

Palmer, T. N. (1982). Properties of the Eliassen-Palm flux for planetary scale motions. *J. Atmos. Sci.*, *39*(5), 992–997. https://doi.org/10.1175/1520-0469(1982)039<0992:POTEPF>2.0.CO;2

Park, J. S., Park, S. H., Chun, H. Y., Yoo, J. H., and Shin, U. (2024). Analysis of planetary scale waves using Idealized sudden stratospheric warming simulations in different dynamical cores. *J. Geophys. Res.: Atmos.*, *129*(6), e2023JD039703. https://doi.org/10.1029/2023JD039703

Rezac, L., Jian, Y., Yue, J., Russell III, J. M., Kutepov, A., Garcia, R., Walker, K., and Bernath, P. (2015). Validation of the global distribution of CO_2 volume mixing ratio in the mesosphere and lower thermosphere from SABER. *J. Geophys. Res.: Atmos.*, *120*(23), 12067–12081. https://doi.org/10.1002/2015JD023955

Salby, M. L. (1981). The 2-day wave in the middle atmosphere: observations and theory. *J. Geophys. Res.: Oceans*, *86*(C10), 9654–9660. https://doi.org/10.1029/JC086iC10p09654

Salby, M. L., and Callaghan, P. F. (2001). Seasonal amplification of the 2-day wave: Relationship between normal mode and instability. *J. Atmos. Sci.*, *58*(14), 1858–1869. https://doi.org/10.1175/1520-0469(2001)058<1858:SAOTDW>2.0.CO;2

Shepherd, M. G., Wu, D. L., Fedulina, I. N., and Gurubaran, S. (2008). Temperature variability in the tropical mesosphere during the northern hemisphere winter. *Adv. Space Res.*, *41*(9), 1435–1446. https://doi.org/10.1016/j.asr.2007.04.035

Shepherd, M. G., Beagley, S. R., and Fomichev, V. I. (2014). Stratospheric warming influence on the mesosphere/lower thermosphere as seen by the extended CMAM. *Ann. Geophys.*, *32*(6), 589–608. https://doi.org/10.5194/angeo-32-589-2014

Shepherd, T. G. (2007). Transport in the middle atmosphere. *J. Meteor. Soc. Jpn., 85B*, 165–191. https://doi.org/10.2151/jmsj.85B.165

Smith, A. K., Marsh, D. R., Mlynczak, M. G., and Mast, J. C. (2010). Temporal variations of atomic oxygen in the upper mesosphere from SABER. *J. Geophys. Res.: Atmos., 115*(D18). https://doi.org/10.1029/2009JD013434

Solomon, S., Plattner, G. K., Knutti, R., and Friedlingstein, P. (2010). Irreversible climate change due to carbon dioxide emissions. *Proc. Natl. Acad. Sci. USA*, *106*(6), 1704–1709. https://doi.org/10.1073/pnas.0812721106

Tassev, Y. K., Spassov, H. V., and Vellinov, P. I. (1993). On the relationships between vertical ozone distribution and middle atmosphere dynamics during stratospheric warming at solar minimum. *Adv. Space Res.*, *13*(1), 321–324. https://doi.org/10.1016/0273-1177(93)90030-f

Vallis, G. K. (2017). *Atmospheric and Oceanic Fluid Dynamics* (2nd ed). Cambridge: Cambridge University Press.

Vignon, E., and Mitchell, D. M. (2015). The stratopause evolution during different types of sudden stratospheric warming event. *Climate Dyn.*, *44*(11–12), 3323–3337. https://doi.org/10.1007/s00382-014-2292-4

Wade, M., Rodríguez-Fonseca, B., Martín-Rey, M., Lazar, A., López-Parages, J., and Gaye, A. T. (2023). Interdecadal changes in SST variability drivers in the Senegalese-upwelling: the impact of ENSO. *Climate Dyn.*, *60*(3–4), 667–685. https://doi.org/10.1007/s00382-022-06311-3

Wang, J., Zeng, N., Wang, M. R., Jiang, F., Chen, J. M., Friedlingstein, P., Jain, A. K., Jiang, Z. Q., Ju, W. M., … Wiltshire, A. J. (2018). Contrasting interannual atmospheric CO_2 variabilities and their terrestrial mechanisms for two types of El Niños. *Atmos. Chem. Phys.*, *18*(14), 10333–10345. https://doi.org/10.5194/acp-18-10333-2018

Wu, D. L., Hays, P. B., and Skinner, W. R. (1995). A least squares method for spectral analysis of space-time series. *J. Atmos. Sci.*, *52*(20), 3501–3511. https://doi.org/10.1175/1520-0469(1995)052<3501:ALSMFS>2.0.CO;2

Yamazaki, Y., Matthias, V., and Miyoshi, Y. (2021). Quasi-4-Day wave: Atmospheric manifestation of the first symmetric Rossby normal mode of zonal wavenumber 2. *J. Geophys. Res.: Atmos.*, *126*(13), e2021JD034855. https://doi.org/10.1029/2021JD034855

Yasui, R., Sato, K., and Miyoshi, Y. (2021). Roles of Rossby waves, Rossby–gravity waves, and gravity waves generated in the middle atmosphere for interhemispheric coupling. *J. Atmos. Sci.*, *78*(12), 3867–3888. https://doi.org/10.1175/JAS-D-21-0045.1

Yoo, J. H., and Chun, H. Y. (2025). Role of in situ-excited planetary waves in polar vortex splitting during the 2002 Southern Hemisphere sudden stratospheric warming event. *Atmos. Chem. Phys.*, *25*(20), 13651–13664. https://doi.org/10.5194/acp-25-13651-2025

Yoshida, K., and Yamazaki, K. (2011). Tropical cooling in the case of stratospheric sudden warming in January 2009: focus on the tropical tropopause layer. *Atmos. Chem. Phys.*, *11*(13), 6325–6336. https://doi.org/10.5194/acp-11-6325-2011

Yue, J., and Gan, Q. (2021). Quasi-two-day wave modulation of carbon dioxide in the mesosphere and lower thermosphere. *J. Atmos. Sol. Terr. Phys.*, *224*, 105750. https://doi.org/10.1016/j.jastp.2021.105750

Zhang, C. Y., Zhang, J. K., Maycock, A. C., and Tian, W. S. (2024). Distinct tropospheric anomalies during sudden stratospheric warming events accompanied by strong and weak Ural Ridge. *NPJ Climate Atmos. Sci.*, *7*(1), 280. https://doi.org/10.1038/s41612-024-00826-8

Zhang, X., Nakazawa, T., Ishizawa, M., Aoki, S., Nakaoka, S. I., Sugawara, S., Maksyutov, S., Saeki, T., and Hayasaka, T. (2007). Temporal variations of atmospheric carbon dioxide in the southernmost part of Japan. *Tellus B: Chem. Phys. Meteor.*, *59*(4), 654–663. https://doi.org/10.1111/j.1600-0889.2007.00288.x